Iterative Learning Control Algorithm for Greatly Increased Bandwidth and Linearity of MEMS Mirrors in LiDAR and Related Imaging Applications

Veljko Milanović*, Abhishek Kasturi, Hong Joo Kim, Frank Hu

Mirrorcle Technologies, Inc., Richmond, CA

ABSTRACT

Gimbal-less dual axis point-to-point (quasistatic) MEMS mirrors have very wide bandwidths for laser beam steering, however users are often limited to only a third of the bandwidth due to the high Q-factor and use of low-pass filters in open-loop operation to avoid overshoot and oscillation. Closed-loop driving enables the use of the full bandwidth with additional complexity in optics and electronics, which can be undesirable in some low SWaP-C systems [3]. But for many applications which require scanning repetitive patterns, such as LiDAR and biomedical imaging, bandwidth utilization and linearity can be greatly increased without any real-time feedback control by training the device and finding an optimal driving waveform using an iterative learning algorithm.

The algorithm drives the device with a trial waveform, measures the scan on a Position Sensing Device (PSD), calculates the error between the desired waveform and the measured position, and adjusts the drive waveform for the next iteration based on an approximate linear device model. This is repeated until the error is reduced to below an acceptable specification. The waveform is then saved in the MEMS Controller and can be reliably used for extended periods of operation. Multiple such drive signals can be trained and stored on the controller to perform different types of scans.

Several MEMS mirrors, including single- and dual-axis designs, were studied and three are reported here. Overall, in all cases a high accuracy of optical scans is achieved, typically to within ±0.025° of nominal. Repeatability after training, then running in open loop is better than ±0.01° - however, this measurement was limited by the lower resolution of the position detecting sensor. Scan rates achieved vary based on mirror design, but in each case are greatly improved from those achievable with basic driving approaches [3]. Each mirror demonstrated higher quality vector graphics content at faster refresh rates and stable linear rasters at rates below resonance where lines are scanned with uniform velocity. Additionally, each mirror could achieve stable fast rasters with the line-scanning axis rates just below resonance, giving sinusoidal scans with line rates of ~1.6f_{res}. Finally, each mirror was also demonstrated achieving rasters with rates above resonance, giving line rates of ~2.5f_{res}. In all of those cases the other axis could scan linear and sharp sawtooth or triangle waveforms. Based on the symmetry of the MEMS design, we demonstrated the same performance at different angles, e.g. rastering at a 45° angle.

Keywords: MEMS mirror, iterative learning control, solid state LiDAR, handheld OCT probe, dynamic headlight, dynamic solid state lighting, picoprojector, retinal projection.

1. INTRODUCTION
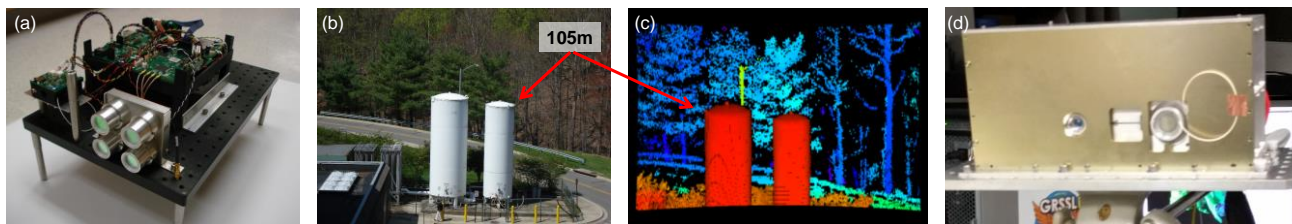
1.1 MEMS MIRRORS IN LIDAR APPLICATIONS

Figure 1. (a) Army Research Lab's duo-static LiDAR system using a gimbal-less MEMS mirror to scan the laser over a wide field of regard (FoR) [2], (b) and (c) are photographs of the LiDAR's FoR and the resulting image of the LiDAR scan, clearly identifying objects 105m away and low-reflectance tree canopies beyond that, (d) a prototype LiDAR developed by NASA GSFC dubbed Goddard Reconfigurable Solid-state Scanning Lidar (GRSSLi) using gimbal-less mirrors [5].

LiDAR technology is widely utilized in optical sensing applications, such as advanced driver assistance systems (ADAS) and unmanned ground and air vehicle systems (UGV, UAV). A major segment of the emerging LiDAR technology relies on beam steering capabilities of MEMS mirrors to satisfy scanning parameters for a required field of regard (FoR) [1]. MEMS mirror technology is chosen particularly because of its compact nature, low power consumption, and potential for low-cost mass production. Research labs and a number of companies have utilized both single and two-axis design Mirrorcle MEMS mirrors as their beam steering components to scan fast, repetitive waveforms. As an example, the Army Research Laboratory (ARL) has utilized Mirrorcle gimbal-less two-axis 1.2mm diameter MEMS mirrors (A3I12.2-1200AL), along with a wide-angle projection lens and aperture for reflected light, for laser beam steering based LiDAR (Figure 1a-c), developed for UAV and other defense applications [2][3]. In later versions, focused on longer distance and higher average power, 2.0mm and 2.4mm diameter mirrors were proven to be more effective while still easily providing the necessary linear raster rates. Boeing Spectrolab has also utilized gimbal-less mirrors in the transmitter section of its scanning LiDAR camera, SpectroScan 3D [4]. Another example, based on the reference design presented by ARL, is NASA Goddard's 3D-Imaging LiDAR dubbed Goddard Reconfigurable Solid-state Scanning Lidar (GRSSLi) (Figure 1d), which is primarily being designed for space-based applications [5]. In these LiDAR applications, waveforms are practically in every case known *a priori* and repetitive in nature, allowing for device optimization and training prior to product integration and deployment. While the beam steering requirements can be very demanding, the fact that the scan patterns are known and can be optimized *a priori* provides a major advantage for the technology. Of course the solution must then rely on extremely repeatable (over time and temperature) MEMS mirrors such as the silicon-based electrostatic gimbal-less dual-axis MEMS mirrors [3][14].

1.2 PROGRAMMABLE LIGHT SOURCE TECHNOLOGY AND DYNAMIC AUTOMOTIVE HEADLIGHTS

Solid-state lighting (SSL) has become the go-to lighting technology due to many significant advantages over traditional approaches, including better efficiency, longer lifespan and modularity. The highest efficiency and overall brightness in lighting is achieved with light emitting diode (LED) solid-state sources used in conjunction with phosphors for wavelength conversion and light diffusion. Recently, another form of SSL technology is gaining momentum and attracting more attention – laser phosphor lighting. In this variant of the SSL technology, the solid-state LED source is replaced by a laser diode (LD). Because the laser diode has a much lower Etendue (emission from a much smaller area in narrower angle) and is more coherent, it allows for better control, shaping, and focusing of the source on the phosphor plate, e.g. provides the option to illuminate a tiny spot on the phosphor plate [23]. This results in an extremely high luminous intensity per unit area (or luminance, Cd/m^2) which has several advantages for lighting designers. One advantage is that the resulting light can be very efficiently directed, shaped and confined to a narrow cone of angle for long-distance lighting applications while employing smaller and lower-cost optics.
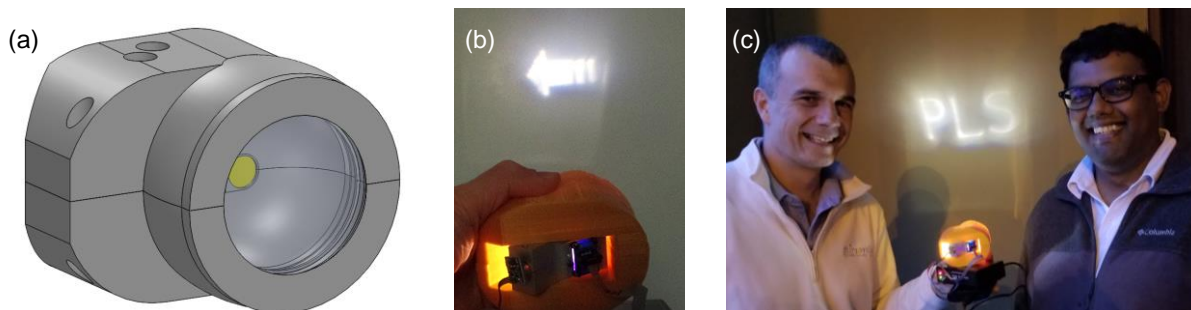

Figure 2. Programmable Light System (PLS) Prototype: (a) 3D model of the PLS prototype with the phosphor plate visible behind the projection lens, (b) Example of a linear raster scan to project an image of a directional arrow as white light content, (c) Authors demonstrate a battery-powered prototype, displaying vector content to maximize brightness.

Automotive headlight developers increasingly utilize laser-based lighting, benefiting from its capability to produce much higher luminance at a fraction of the size, weight and energy efficiency of LED headlights [7]. Next generation automotive headlights target the inclusion of dynamic functions, effectively turning the headlight into a white-light projector display. Recent development aims at systems capable of projecting programmable content ahead of vehicles utilizing high power, focused laser beams onto phosphor conversion plates. A beam-steering MEMS mirror enables such a display projector in automotive laser headlights. The luminance of laser headlights, combined with MEMS mirrors' ability to scan waveforms with fast and accurate point-to-point scanning, can be used to e.g. selectively illuminate obstacles or traffic signs, reduce illumination directed towards oncoming traffic, or project vector content like turn

signals on the road to assist the driver. In such a dynamic solid-state lighting (DSSL) system, which we termed Programmable Light Source, MEMS mirrors can programmably illuminate the remote phosphor target while offering small form factor, low cost and power consumption.

We have demonstrated such dynamic, solid state lighting prototypes in 2016 [6] based on both transmissive and reflective mode arrangements, and stressed the advantages of utilizing point-to-point (or quasistatic) MEMS mirrors to obtain efficient utilization of available laser power and highest luminous emittance. Compared to area-based imaging systems such as picoprojector-based solutions (source is turned off a significant portion of the time) or DLP-based solutions (significant non-projected portion of the light is dumped as heat into the system), this approach results in dramatically better efficiency and luminous emittance. Recently we have improved the designs and demonstrated both raster-based displaying methodology, as well as vector content displaying based on the same system (Figure 2). This capability would allow projection of programmable lighting for a variety of industrial and ultimately consumer applications.

Scans for many lighting functions would be known *a priori* and can therefore be optimized during system integration/production. For some real-time reconfigurable cases where lighting content must respond to sensor input for example (security system spotlights) – the optimization cannot be generally performed. However, even in such cases most of the patterns and symbols could be initially trained and optimized only to be later manipulated in projection based on size, offset, or rotation for example.

1.3 MEMS MIRRORS IN MEDICAL IMAGING APPLICATIONS

Optical coherence tomography (OCT) is used in biomedical imaging instruments, as a non-invasive imaging technique used to visualize cross-sections of biological specimen. The medical imaging industry relies on OCT and related imaging modalities when rapid microscopic point-of-care (POC) imaging of a non-prepared specimen is needed. Beam steering is critical in such imaging systems; it enables fast and accurate point-to-point scanning of laser light onto the specimen and gathering of backscattered light back to the sensor. Linear raster capability with uniform velocity scans across the specimen is typically preferred, as shown in a simple example of Figure 3a. Namely, uniform velocity scans allow equal time of exposure and measurement at each pixel which improves overall quality of the image.

Recently, MEMS mirrors have replaced galvanometers as the go-to choice for handheld (portable) optical scanners; they utilize orders of magnitude less driving power and provide fast two-axis optical beam scanning at a fraction of the size, weight and cost of galvanometer-based systems [8][9][10]. Companies such as Santec Corporation, Wasatch Photonics, and others have all implemented Mirrorcle MEMS gimbal-less two-axis mirrors in their respective small form factor OCT scanning hardware, and have taken advantage of these mirrors' arbitrary control of scan area and beam velocity, small size and low power consumption. Figure 3b shows another excellent example of Thorlabs handheld probe part OCTH-900 and OCTH-1300 [11] where the mirrors are utilized either in single-axis (b-scan) mode, or in dual-axis (b and c scan) mode.

Figure 3. (a) Example of a linear raster scan that can be optimized for a MEMS mirror by training the device in iterative learning, and be driven in open loop, (b) example of a bio-medical imaging handheld scanner that uses a gimbal-less, dual-axis MEMS mirror, Thorlabs part OCTH-900.

The above-mentioned linear rasters require wide bandwidth MEMS actuation and can be challenging for larger diameter MEMS mirrors which are frequently preferred to increase sensor resolution. However, in current MEMS mirror-based OCT scanners, waveforms are practically always known *a priori*. The typical target for the probe designer is to rapidly scan over the target specimen with high repeatability. Furthermore, constant velocity or point-to-point scanning is often desired, with a typical scan as schematically outlined in Figure 3a. Those requirements are met more easily if the waveforms are optimized for the specific beam steering element ahead of time, during product integration/production or

calibration. Even if several different scan functions are to be performed by the probe, each of those could be efficiently trained and optimized during production and stored in the hardware.

1.4 MEMS MIRRORS IN LASER PROJECTOR DISPLAYS

Battery-powered 'picoprojector' systems based on (RGB) lasers as light sources have been available for many years, although the overall technology is still in development toward better performance specifications and cost. More recently the push for retinal displays in AR/VR hardware has re-invigorated compact laser-projector development. In such cases we often utilize two single-axis mirrors to produce distortion-free wide-angle scans to generate very sharp and stable image of e.g. 1280 x 720 pixel resolution to be delivered to a display surface or a human eye.

From a technology standpoint, it is relatively easier to realize a single axis mirror that resonates at high speeds to 'draw' a line onto the projection screen. This line that is generated by the 'fast axis' scan axis then needs to be pointed in a quasistatic (point-to-point) fashion to be distributed on the other axis, to cover a full 2D area. This is a more complex requirement demanding not only an extremely repeatable point-and-stop movement for the amount of lines a system is laid out to be, but also to 'hop back' to the first line once a full rectangle has been completed. The tendency of refresh rate requirements for this "slow" axis is to increase, from 60Hz to 90Hz and then 120Hz, and therefore the challenge certainly remains [22]. This mirror can greatly benefit from iterative 'training' to optimize its speed, angle, and linearity. Ultimately both the resonant and quasistatic axis can be trained for best overall results.

Figure 4 shows a prototype projector with two single-axis mirrors. Single-axis resonant mirrors with 21kHz and 24kHz resonant frequencies and angles of $\pm7.5°$ or larger are utilized in the prototypes. The 2nd mirror is rectangular (4mm x 1.3mm) with a very wide bandwidth quasistatic capability to run 60Hz, 90Hz, or even 120Hz sawtooth waveforms with fast retrace. First mirror can also have a larger diameter for some special imaging cases where beam divergence must be reduced. A 1mm diameter resonant mirror with approx. 15kHz resonance is used in that case or a 1.2mm resonant mirror with ~12.8kHz resonance. All of these options, when combined with the A9Q40 rectangular mirror can achieve extremely repeatable high refresh rate raster scans for a variety of imaging or display applications.
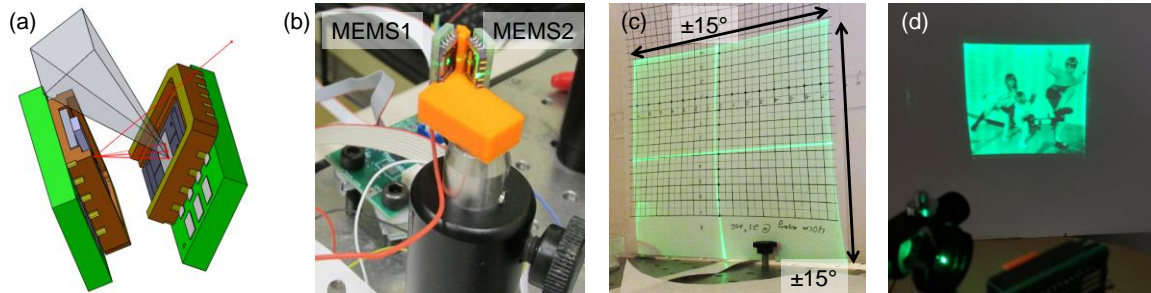

Figure 4. MEMS mirror based Laser Projection Technology. (a) a 3D-model depiction of the MEMS mirror based pico-projector using two single axis mirrors (2SA), showing the path of the laser beam reflecting from MEMS1 (resonant X axis) to MEMS2 (Quasistatic Y axis), and the final image projection field of view, (b) 3D-printed prototype of the PicoProjector demonstration, using a single color, 520nm laser, (c) the projector is capable of scanning with ±15° optical field of view, (d) an example of pico-projection by displaying a 600 x 600 pixel image in 8-bit gray scale, using a 520nm laser.

1.5 PRIOR WORK ON INCREASED BANDWIDTH AND LINEARITY

In 2017, we presented work on extending the bandwidth and controlling the resonant frequency response of MEMS mirror devices by applying a number of different open-loop and closed-loop methodologies [3]. A case example studied was the 2mm mirror A7M20.1 with the first resonance at ~1.3kHz and $\pm5°$ point-to-point mechanical angle. In the simplest methodology, a low pass filter (LPF) was implemented in series with the drive signal for the MEMS device in open-loop operation, resulting in a -3dB point in overall response (magnitude) of approximately 500Hz, or about $0.4f_{res}$, where f_{res} represents the device's first resonant frequency. The device was able to perform relatively linear scans of 100Hz triangular waveforms, but with some distortions (reduced linearity). An inverse system filter, based on a second-order linear time invariant (LTI) model of the MEMS device, was applied to extend the bandwidth to 1.2kHz, approximately $0.92f_{res}$. In that case, 200Hz triangle waveforms were scanned with near-maximum linearity at mechanical angles of +/-3° but not at full mechanical angles of $\pm5°$, where distortions were again observed. When a proportional-integral-derivative (PID) controller was used, resonant response was fully suppressed, and bandwidth was extended to

$1.25f_{res}$, resulting in linear scans of 200Hz triangle waveforms at full mechanical angles (±5°). Higher gains on the PID controller further extended the bandwidth to approximately $3f_{res}$, greatly beyond the device's resonant frequency, and scans of 500Hz and 1kHz triangle waveforms achieved considerable linearity at full mechanical angles [2].

1.6 GOAL OF THIS WORK

Presented above are various beam-steering applications where a MEMS mirror is typically driven by predetermined content stored in memory, such as linear raster scans. For these cases, we have been investigating learning-type training and/or control algorithms such as iterative-learning-control (ILC), repetitive control (RC), and related techniques to train MEMS mirrors so that they can perform faster and more linear scans. This implementation would allow for increased bandwidth and linearity, and only require a relatively simple optical setup and driving electronics without real-time control capability. Moreover the setup would be only required at the time of manufacture or initial training and not in application, giving the better results in application without additional complexity. This paradigm would of course rely on the high repeatability and stability of electrostatic gimbal-less MEMS mirrors over time, temperature, and other environmental conditions. Once the desired waveform is determined via these algorithms, it is saved and flashed to the MEMS Controller's memory, and the MEMS devices are driven in open loop with high repeatability for extended periods of time. This excellent repeatability is owed to pure single-crystal silicon construction and electrostatic driving.

An approach toward the related goal was previously developed and presented by Giannini *et al* [12] for use with single-axis MEMS mirrors, to increase their bandwidth and improve their scan accuracy. In that work, a time-domain based convolution-deconvolution approach was used, and after performing a few thousand iterations authors achieved significant improvements in linearity and accuracy of very fast scans. Their method utilizes a masked or cropped waveform approach, focusing only on critical portions of the scan for optimization. In this work, our goal is to utilize frequency-domain based (filtering) methodology based on inverse system model, to optimize complete waveforms (from start to end), and to achieve convergence to acceptable errors in tens of iterations.

2. EXPERIMENTAL SETUP
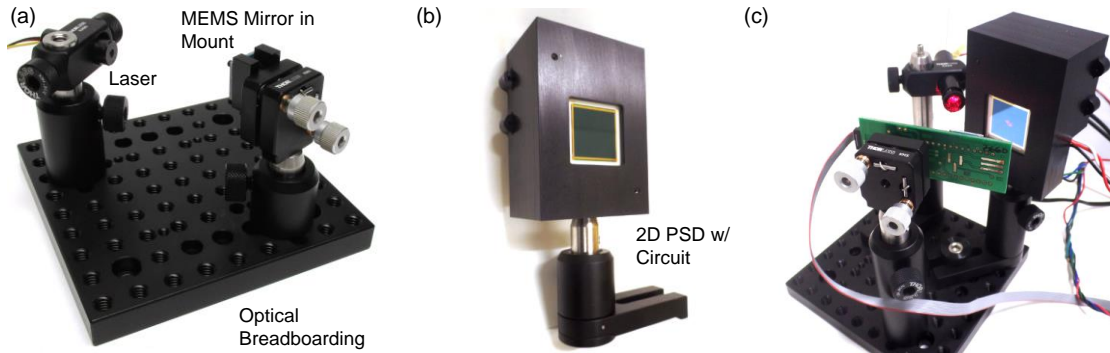
2.1 OPTOMECHANICAL SETUP

Figure 5. (a) Optical breadboarding components for mounting a laser and MEMS mirror from a Mirrorcle MEMS Standard Development Kit [15], (b) Position Sensing Device (PSD) with circuit and mechanical mount, (c) The combined optomechanical setup used in this experiment.

This experiment's optomechanical setup was implemented using standard optical breadboard parts (Figure 5a), chosen for their flexibility to adjust the setup as needed [15], with the additional position sensor module as an add-on (Figure 5b). The setup (Figure 5c) consists of an optical breadboard, a MEMS mirror in a kinematic mount, a focusable, 635nm laser and a Position Sensing Device (PSD) Module. The PSD Module includes a 20mm duo-lateral PSD (DL400-7 PCBA from First Sensor) with transimpedance amplifiers, summing and difference amplifiers and a divider circuit. The module outputs X and Y positions of the laser beam on the PSD, represented as voltages in the -10V and +10V range (corresponding to -10mm to +10mm position, respectively). The MEMS mirror is placed approximately 30mm away from the PSD, and the laser beam is incident onto the MEMS mirror at 20° to minimize optical distortions. The distance to the PSD is determined by a mirror's maximum optical scan angle, such that the scanned laser beam fits onto the 20mm x 20mm sensor (Figure 5c). The MEMS mirrors in this experiment range from ±5° to ±7.5° mechanical angle (next

section). The MEMS mirror and PSD Module connect to the USB-SL MZ MEMS controller or the OCCIE 1.1 MEMS controller (see Sec. 2.4). To ensure accurate reading during testing and operation, ambient light is eliminated. Experiments are conducted in a dark room or with a cover over the optomechanical setup.
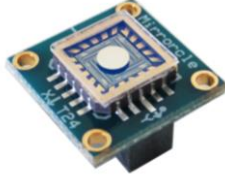
2.2 SELECTION OF MEMS MIRRORS

MEMS Mirror P/N	A7M20.1-2000AL-TINY20.4-NW	A7B1.1-3000AL-TINY20.4-B/EP	A8L2.2-4600AU-TINY48.4-A/EP
Mirror Size	2.0mm	3.0mm	4.6mm
Mech. Angle	±5.0°	±7.5°	±5.0°
Freq. of 1ˢᵗ Resonance	1300 Hz	425 Hz	330 Hz
Freq. of 2ⁿᵈ Resonance	N/A	1050 Hz	1500 Hz
Conn. Package Size	15mm x 15mm	15mm x 15mm	20mm x 15mm

Figure 6. A table of the three gimbal-less dual-axis MEMS device designs reported in this study.

Three different MEMS devices are reported from the study, as detailed in Figure 6. All three MEMS mirrors are designed for two-axis quasistatic (point-to-point) beam steering. Many other designs and products including a single-axis mirror A9S1.1-E3100 (3.1mm x 2.0mm elliptical mirror) were used in selected tests but are not reported here. The devices studied herein were selected based on their scan angle capabilities, mirror diameters, device bandwidths and package sizes, key parameters to determine potential use in specific applications. For example, the 2.0mm mirror fits the needs of the dynamic lighting applications; the mirror can withstand the high laser power of a 450nm laser while offering sufficient bandwidth to display text and other vector content. Furthermore, it can be used in duo-static LiDAR designs with longer distance capability (>150m). In handheld biomedical applications, the compact size of the MEMS mirror with a relatively large mirror diameter and large angle can maximize the imaging capability. Mono-static LiDAR applications are typically photon starved, requiring a large diameter mirror to scan the laser over the FoR, and receive enough reflected light back for accurate time of flight (ToF) measurements. These devices are characterized on a MEMS characterization station that calibrates and determines key characteristics such as static (DC) response, small-signal frequency response, step response and a two-dimensional look-up-table (LUT).

2.3 MEMS DRIVERS

To ensure proper driving of Mirrorcle's gimbal-less MEMS mirrors, several hardware solutions are available [13] tailored to the specific needs of various applications. They ensure finely controllable tip/tilt movement of the MEMS mirrors to large angles. Hardware options range from basic drivers that take low voltage analog signals or digital SPI signals to convert to high voltage MEMS drive signals, to more complex controllers with microcontrollers or FPGAs. The diagram in Figure 7 depicts various layers of integration that may appear in typical MEMS scanning applications. The lowest recommended level of integration in applications is to use the MEMS mirror with a designated driver to provide properly conditioned voltage signals. These drivers are the lowest level of electronics integration and require users to supply suitable X and Y position voltages or signals, power, ground and a TTL clock signal for low pass filters.

The driver footprint was recently reduced to 35mm x 40mm x 9mm. These drivers are optimized to safely drive MEMS mirrors and include programmable 5th order low-pass filters (LPF) for smoothing output voltages, a high voltage DC/DC circuit and a high voltage amplifier. The drivers output two bias-differential pairs (four total channels) that range from 0V to 200V, allowing for Vbias voltages up to 100V. These MEMS drivers require only +5V DC voltage supply and consume approximately 70mW of power, making them especially suitable for battery-powered or portable applications. The bandwidth of the standard drivers is up to 25kHz, however, in actual applications, the bandwidth is determined by the user-set LPFs which should match an individual MEMS mirror's recommended filter cut-off setting as defined in its datasheet.
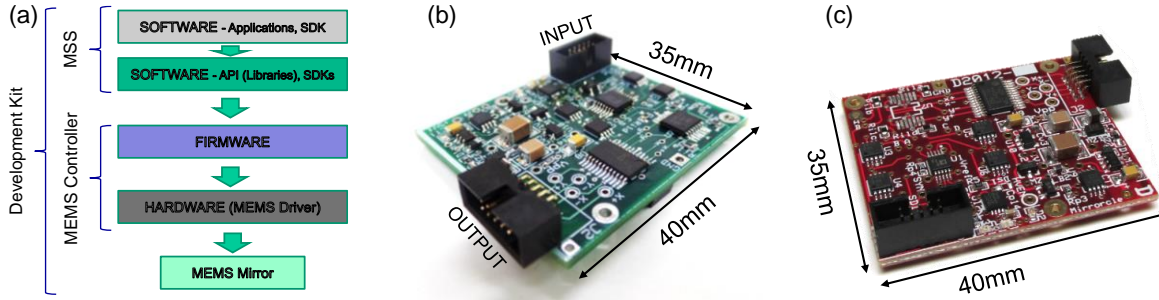
Figure 7. MEMS Mirror control and driving overview: (a) Layers of integration from software layer with user/system command of mirror movement all the way down to the MEMS Driver electronics and finally the mirror itself. (b) MEMS driver – analog input for driving of electrostatic gimbal-less dual-axes MEMS mirrors.(c) A variant of the same MEMS driver with digital input (SPI based).

2.4 CONTROLLERS

For applications that require a higher level of integration, Mirrorcle's USB-SL MZ controllers have an embedded MEMS driver similar to the ones described in the driver section (2.3), along with a microcontroller (Microchip part PIC32MZ) to provide higher level functions. The MCU enables the user to communicate with the software level to download and run custom content, flash waveforms to memory and programmability to boot up and run waveforms without any additional hardware interface. These Controller boards customarily ship with the company's plug-and-play development kits. They are USB-powered and –controlled, and offer ready-to-use control electronics to allow for instant experimentation with MEMS mirrors using Windows applications [15]. The controllers also have APIs available on several different development platforms – namely C++ (Windows and Linux), LabView and MATLAB SDKs as well as Java (Android) SDK.

The established USB-SL MZ Controller is pictured in Figure 8b. The controller weighs ~140g and comes in a compact 80mm x 115mm x 30mm box with labeled connectors and status signal LEDs. Along with the MEMS driving capabilities, the controller also has two analog inputs that accept ±10V inputs, 8 channels of correlated digital outputs to trigger additional controllers or driving of lasers, cameras or other peripherals, a synchronization port that can either send or receive external triggers or clocks, and a sensor port to connect a photodiode for tracking and imaging applications. The most recent generation of the MEMS Controllers (Figure 8c) is a more compact version, approximately 40mm x 70mm x 10mm, offering the same mirror control and peripherals as the 'standard' Controller.
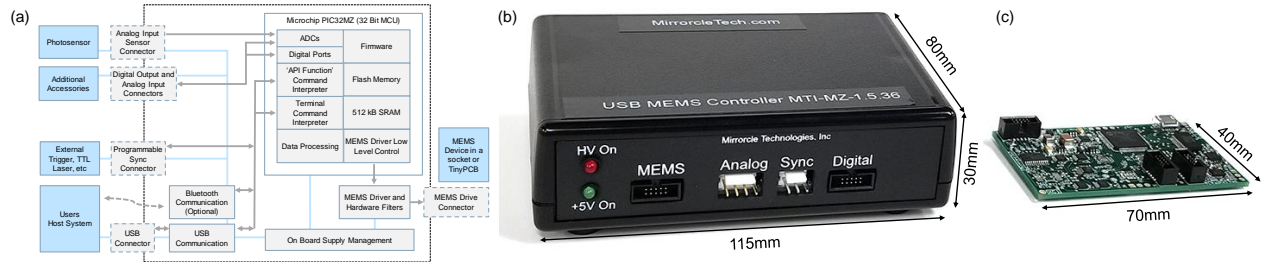

Figure 8. USB MEMS Controller used in this project based on Microchip's PIC32MZ MCU and MEMS driver: (a) Block diagram of the Controller, (b) Box version of the USB-SL MZ Controller with easily accessible ports for a variety of possible connections and quick prototyping, (c) Compact version of the controller OCCIE 1.1 with full functionality with consolidated ports for OEM development and integration into applications.

3. LEARNING CONTROL FOR TRAINING OF MEMS MIRRORS

Iterative Learning Control (ILC) is a methodology for improving control in mechanical applications and systems where repetitive (actuation) work is performed, for example when repeating or periodic laser beam scanning is required [16][17][18]. Examples of systems include robot arm manipulators, laser beam scans in material processing or imaging, etc. In these types of systems, the actuator is required to accurately perform the same action over and over. Accuracy of the performed action is one important parameter, but the speed is often another critical parameter which can be improved

with ILC. Iterative learning control (ILC), repetitive control (RC), run-to-run control (R2R) and a number of related learning-type control methodologies were all proposed in different fields, to address different problems, and have a number of similarities and some distinct differences [18].

Methodology used in this work follows the general principles but may differ in the fact that an approximate inverse system model is used to obtain a correction factor for subsequent iterations. Initially, we define target scan (beam position vs. time) as the set point signal (as in closed-loop control systems) or *S*. This set point waveform is determined over a finite time interval and may require the system to perform it over and over periodically, but it could also be triggered one or more times non-periodically and on command once it has been learned by the system.

The process begins with the assumption that the device is already known from previous characterization procedure in which its voltage to angle response, frequency response, and step response is measured. Thus we can create a simplified linear model of the device H_M. Furthermore the system will perform a simple measurement of time delay in the system hardware (most notably due to hardware filters on the MEMS Controller). This could be defined as the drive system model H_H which in general could be more complex but we found that only the delay term is necessary for good results. The learning algorithm is performed by taking the input waveform I_N, where N represents the iteration number, and providing it as the input into the system, then seeking how to prepare the next iteration I_{N+1} based on the N-th iteration output. We can assume from linear approximation that this input waveform, I, consists of a desired waveform portion G (which the algorithm seeks to find) and an additional portion W which results in output error. An inverse system model, H_M^{-1}, is generated using the MEMS model data and used as a software filter in the initial estimate $I_1 = S * H_M^{-1}$ to reduce the MEMS device's natural response from the drive signal. However the initial estimate can also be a very simple un-optimized guess, e.g. directly proportional to S, simply resulting in more iterations required to settle. The output of the system is the MEMS mirror scan onto the PSD, which is measured as O, or the output waveform. The error signal is calculated as $e_N = S_N - O_N$. To estimate the source of the error e_N in the estimate input I_N, we "pass" the error signal e_N through the approximate inverse system, seeking to find the portion W_N responsible for the error. Thus we obtain an approximate portion $\widetilde{W} = e\, H_M^{-1} H_H^{-1}$. This approximation of the input error $\widetilde{W_N}$ is then fed back into the next iteration's input I_{N+1} by taking the current input of I_N and subtracting the estimated input error $\widetilde{W_N}$ with an error correction gain k.
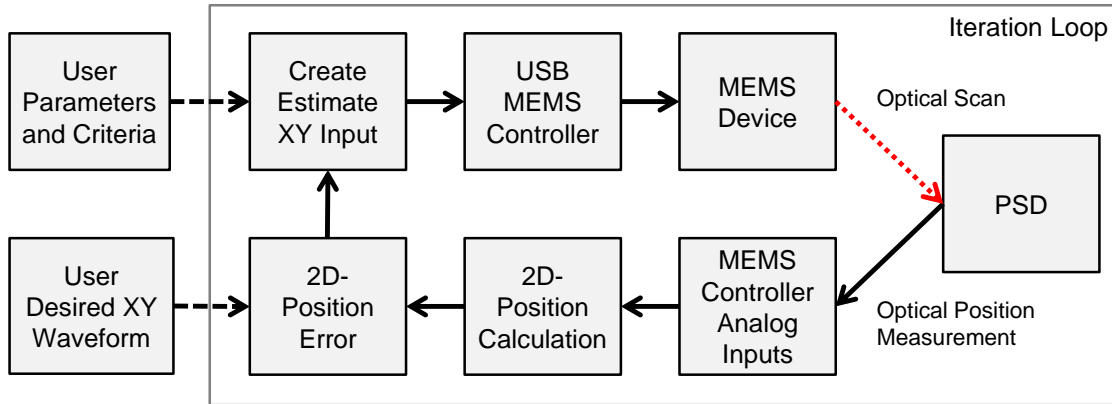

Figure 9. Block diagram of the ILC loop implemented in a Matlab GUI to demonstrate the repeatability of the MEMS mirror. The user has control on various parameters including the number of loops to run, bandwidth of hardware/software filters, error correction gains, etc.

The learning process will attempt to reduce the input error component $\widetilde{W_N}$ during each iteration by using the information gathered from the previous iteration. With the proper hardware settings, input parameters, and output criteria, the result of the learning process will produce a highly optimized output waveform O, which maximizes the set point S, almost eliminating the error e. The error cannot be fully eliminated due to the various analog / digital / analog conversions that happen in each iteration. This learning process is not a control system since each iteration is an estimate calculated from the previous iteration's output, driven in open loop by the MEMS controller, and measured optically on the PSD. The correction gain and user parameters such as the hardware and software filter settings determine how many iterations may be needed to produce an acceptable result. In some cases, there may not be a convergence due to stringent user parameters or high output criteria. Currently, this learning process is implemented using a Matlab GUI, built on the standard development kit controller and its API for software for rapid prototyping and quick implementations of any changes to the iteration loop.

One major advantage of this approach to waveform optimization, leading to higher tracking accuracy is that the iterative process with run to run adjustment allows acausal treatment of waveforms –determination of adjustment at each sample can utilize knowledge of past and future samples – this is of course impossible in real-time (e.g. PID) control loops.

The iterative learning procedure used in this work is customized toward MEMS mirror optimization and includes many parameters which the user can adjust to obtain better results. The set point waveform is fed into the system through a simple text file or through a script to generate a list of sample points. Different attributes are adjustable such as the sample rate, error correction gains, number of iterations, bandwidths of the set point waveforms (X and Y independently), bandwidth of the hardware driver, etc. The iterative process is monitored through a GUI, presenting the user with various graphs such as the waveform being scanned and the error generated in mechanical angle space. The process is repeated to reduce the error from MEMS mirror's output. After reaching an optimized waveform based on the best reduction in the error signal (typically $<\pm 0.01°$ mech. angle) the final drive waveform can be saved or directly flashed to the controller for indefinite open-loop operation. Figure 10 shows the improvement in the raster scan from the second iteration in Figure 10a, fifth iteration in Figure 10b, and the optimized result after 15 iterations in Figure 10c. To test the longevity of this saved scan, some devices have been performing a trained and optimized scan of a 90Hz, 80% sawtooth waveform for +130 days, or ~1 billion scans.
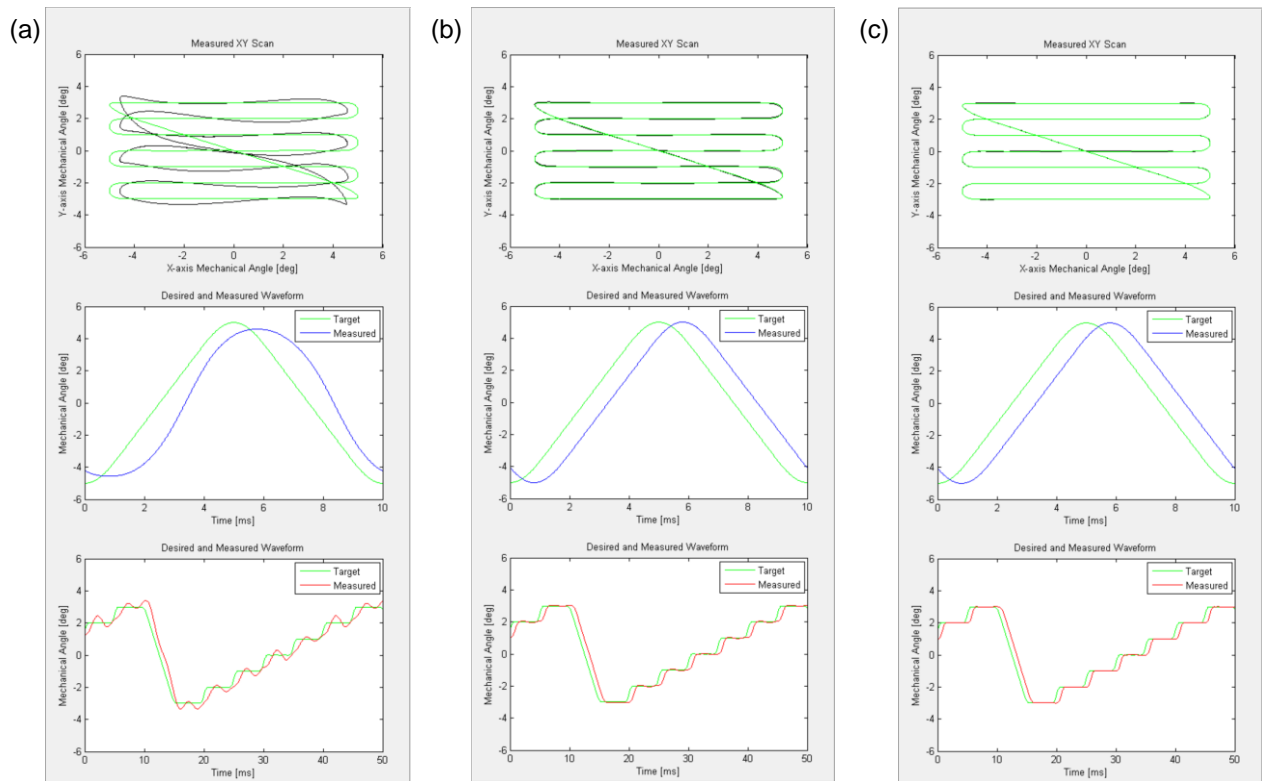

Figure 10. Example of iterative learning progress for the A8L2.2-4600AU device, with an 80Hz by 20Hz raster pattern target with ±5° X-mechanical angle and ±3° Y-mechanical angle for a LiDAR application. The graphs show XY (black), X (blue) versus time and Y (red) versus time plots, compared to their respective set point plots (green). (a) Results after 2 iterations, where both X and Y axes are being excited from resonant frequencies, (b) After 5 iterations, the general raster pattern is resolved on the X axis, with error remaining on the Y axis, (c) After 15 iterations, the complete raster scan is fully resolved with the position error reduced to below ±0.01°.

4. MEMS PERFORMANCE UNDER ILC

To demonstrate increased MEMS performance, we used four types of scanning modes: dual axis point-to-point (quasistatic), linear raster, resonant quasistatic (RQ) raster, and beyond RQ raster. Dual axis point-to-point utilizes the wide bandwidth of operation of a device from DC to some frequency below its resonance to avoid excitation and ringing. Therefore mirror can hold a DC position, or move in a uniform velocity, or perform vector graphics. In linear raster scanning, the fast axis, typically X axis, performs a triangle or sawtooth waveforms, and the slow axis performs a

sawtooth waveform, or sawtooth with discrete steps to define specific lines in the frame. The number of lines in the scan is dependent on the device's bandwidth. The RQ raster is a mixed mode in which one axis is used in quasi-static mode, and the other axis is used in resonant mode. A typical use case is to run a sinusoid waveform on the fast axis to create horizontal lines, and to run the other axis with a sawtooth-like waveform to create a raster pattern that covers a rectangular display or imaging area. The axis operating at resonance should have its parameters carefully obtained to avoid exceeding maximum mechanical angles. Beyond RQ raster mode is an operating mode achievable using learning algorithms or closed-loop control. In this mode, one or both the device's axes scan at frequencies beyond the device's first resonant peak.

The 2.0mm diameter mirror device was used to scan vector graphics through the ILC algorithm. The 40Hz vector scan pattern, "STOP", was generated from our software API and sized to ±3° mechanical angle. It was iterated for 15 iterations until the error was less than ±0.01° mechanical angle as shown in Figure 11a. The integrated 2.0mm mirror is able to scan a pattern of 1200 lines/s (Figure 11b) using the RQ raster mode. Figure 12 shows the results achieved by the 3.0mm bonded mirror, performing the linear raster scan at 180 lines/s and a near RQ raster scan 360 lines/s rates. The RQ and beyond RQ scan modes were demonstrated using the larger 4.6mm mirror with a first resonant peak at 330Hz, shown in Figure 13. The figures below show the measured XY Scan on the first graph, with the individual axes setpoint and measured angles. For Figure 11 and Figure 12, the position error is also presented.
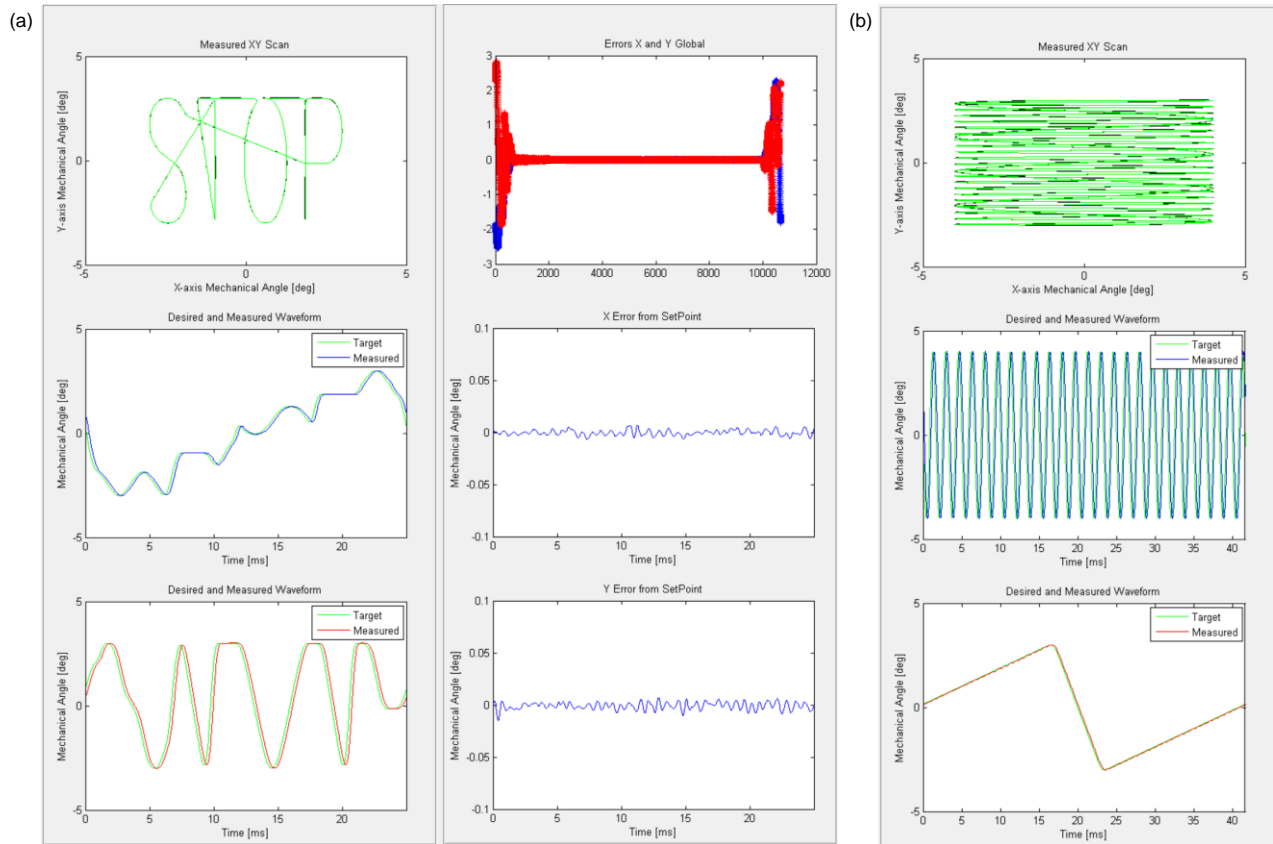

Figure 11. Example of iterative learning for the A7M20.1-2000AL device with patterns controlled under ILC. The first column shows Measured XY Scan (Black) vs. the Set point (Green), X Position (blue) versus time, and Y Position (red) versus time plots compared to their respective set point plots (green) after several iterations. The second column shows the scan's respective error plots, which show position error reduced to below ±0.01°, a) vector scan of the text "STOP" at 40Hz refresh rates, and ±3° X and Y-mechanical angle, b) RQ scan of 600Hz x 24Hz raster pattern at ±4° X-mechanical angle and ±3° Y-mechanical angle, scanning 1200 lines/s.
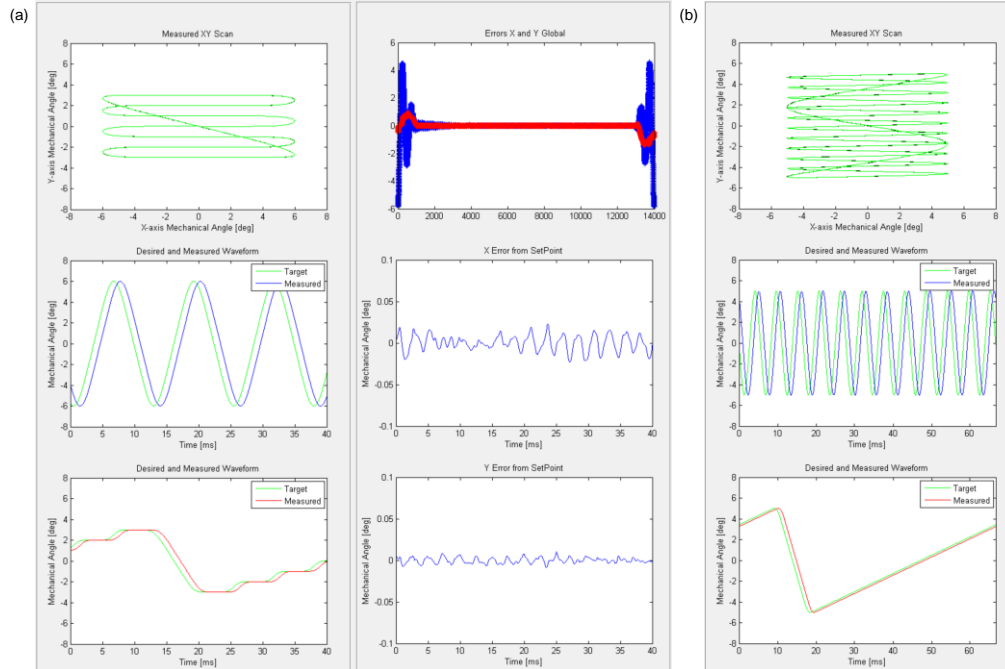
Figure 12. Example of iterative learning for the A7B1.1-3000AL device with a raster pattern target for a LiDAR application: The first column shows Measured XY Scan (Black) vs. the Set point (Green), X Position (blue) versus time, and Y Position (red) versus time plots compared to their respective set point plots (green) after several iterations. The second column shows the scan's respective error plots, which show position error reduced to below ±0.01°, a) A linear raster scan of 80Hz by 20Hz at ±6° X-mechanical angle and ±3° Y-mechanical angle, b) RQ raster scan of 180Hz by 15Hz at ±5° X and Y mechanical angle and 360 lines/s.
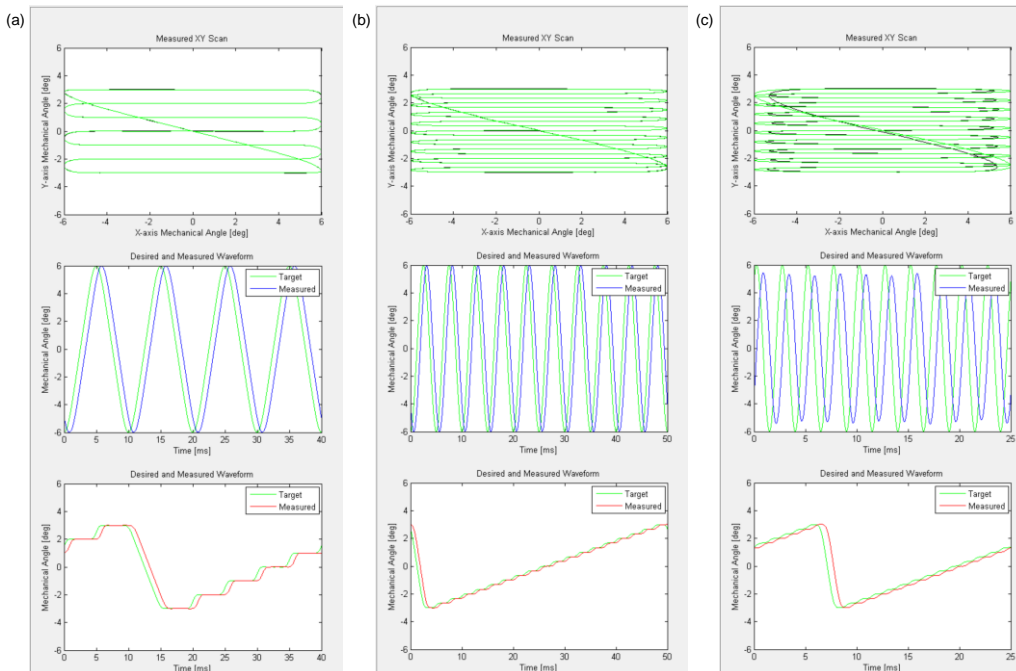

Figure 13. Example of iterative learning for the A8L2.2-4600AU device with a raster pattern target for a LiDAR application: a) A linear raster scan of 100Hz by 25Hz at ±6° X-mechanical angle and ±3° Y-mechanical angle, (b) linear raster scan of 200Hz by 20Hz at ±6 X-mechanical angle and ±3 Y-mechanical angle, (c) A beyond RQ scan of 400Hz by 40Hz at ±5.5° X-mechanical angle and ±3° Y-mechanical angle, scanning 800 lines/s. In this case, the desired angle of ±6° mechanical angle on the X axis was not reached with a convergence in error, therefore stopped at ±5.5°.

5. TECHNOLOGY ROBUSTNESS

A fully calibrated MEMS device can scan an optimized waveform in open loop with the assistance of learning algorithms due to the device's high repeatability and robustness. Mirrorcle MEMS devices have demonstrated 14-bit positional precision on each axis using a 16-bit driver running in open loop. For a device with a mechanical tilt range of -5° to +5°, the tilt resolution is approximately 0.6 milli-degrees or 10 micro-radians. High precision, repeatability and robustness are achieved by the devices due to their pure Single-Crystal-Silicon construction. To reinforce the technology's robustness, we performed various tests on electrical, mechanical and thermal performance, and present them below.

5.1 MECHANICAL SHOCK

In previously presented papers at SPIE conferences, we have presented mechanical vibration and shock testing data of various MEMS mirror devices. Mechanical vibration and variable frequency tests were performed with 20G vibrations from 20Hz to 2kHz, according to MIL-STD-883 Method 2007. All integrated MEMS mirrors were able to pass this specification in tests. The shock tests have been performed in accordance with MIL-STD-883-E, method 2002 [19], testing six axes for 1ms shock at 500G peak and 0.5ms shock at 1500G peak. Additional (in-between) shock increments were added to the test since a wide range of MEMS devices were being tested, and we wanted to see how far certain designs were able to survive. The tests recorded shocks in X and Y-axis first, then a visual inspection is conducted on the devices to optically verify any structural damage, and the Z-axis shock is applied, followed by the visual inspection. The tests began with 300G shock tests, continued to 500G, 1000G and finally 1500G shocks at the end. The integrated MEMS devices in a modified package optimized for damping passed up to 1000G shock in all cases (up to 2.4mm), and 1500G for the smallest mirrors (0.8mm and 1.2mm). A8L1.1 with a bonded 3.0mm mirror passed the 500G at 1ms shock.

5.2 LIFE TIME TESTS

In addition to the mechanical performance qualifications presented, many MEMS devices manufactured over the past decade are still in operation in laboratory settings and in live applications of the technology. Recently, a life time test was put together to test cycles of operation of a MEMS device, operating at higher than rated voltages for the design to stress the devices for an accelerated test. The test uses A5M24.1 integrated MEMS mirror devices, with a 2.4mm Aluminum mirror, in connectorized ceramic packages, scanning a sinusoid waveform at 140Hz, driven by 200V peak-to-peak. The standard A5M24.1 MEMS mirror is rated for 160V peak-to-peak, to reach a maximum angle of approximately ±5.5° mechanical angle. The devices have been running continuously for +170 days, accumulating over 2 billion cycles of movement. The MEMS devices are checked daily for operation, and every other week under a microscope to check for any physical damage to the single-crystal-Silicon MEMS structure. These devices are operating in a clean laboratory setting and with an optical window covering the MEMS device.
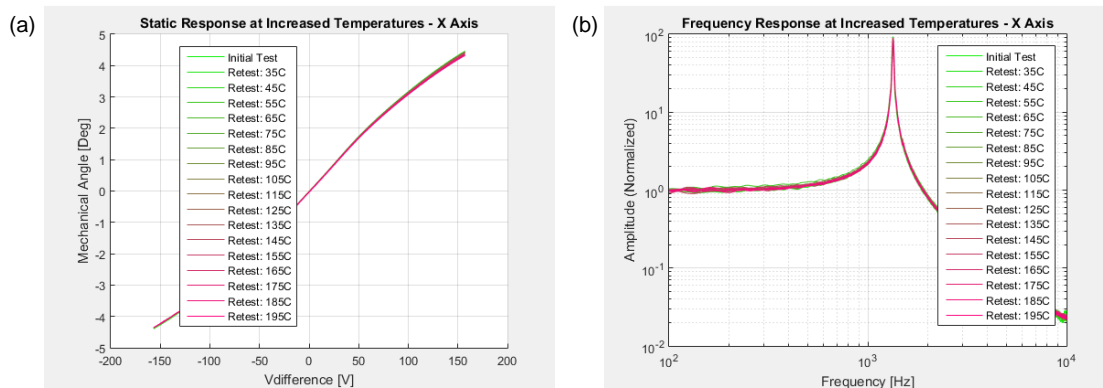
5.3 OPERATION TEMPERATURE

Figure 14. A7M20.1 MEMS mirror (2.0mm Al coated mirror), that is characterized from room temperature of ~25°C up to 195°C in 10°C increments. (a) Static Response shows negligible changes in mechanical angle vs. voltage over a wide range of temperatures, (b) Small Signal Frequency Response of the device shows no changes in resonant frequency or quality factor of the device.

Another important factor in the robustness of the MEMS device is to operate over a wide range of temperatures, with minimal changes to the scan angle and its resonant frequency. Some users of the MEMS mirrors perform calibrations at temperature increments to create LUTs that can be applied to the driver's output to correct for any minor changes in angle. Other organizations have implemented the MEMS mirrors in their own experiments, and have presented work with the device operating at extremely low temperatures of 1 Kelvin [20][21]. Mirrorcle conducted internal tests to characterize the MEMS mirrors at increasing temperatures (up to 200° C) beyond the recommended operating conditions of -40°C to 125°C. An A7M20.1 integrated MEMS mirror device with 2.0mm Aluminum mirror was heated in 10-degree increments from 25°C to 195°C and characterized using standard device characterization test station at each temperature increment. Voltage vs. angle gain showed a minor decrease in total mechanical angle, with 0.14° total decrease on the x axis and 0.09° total decrease on the y axis (Figure 14a). The small signal frequency response presented no inferable trend on either axis (Figure 14b). While the MEMS mirror itself maintains its robustness between -40°C and 195°C, it is not recommended to exceed 150°C in most applications due to limitations on the packaging of the device, in this case the thermal properties of the ceramic package and adhesive.

Additional long-term tests were also conducted to identify contamination and mirror performance after a prolonged thermal bath treatment. Three batches of devices were placed into thermal chambers, and heated on hotplates to 65°C and 105°C temperatures in separate groups, and the third batch of devices at room temperature for control. The devices have been in this study for 2500+ hours and are re-characterized periodically using our calibration test system. The devices are inspected weekly under a microscope and shown to have no issues with contamination or growth. Comparisons in characterization data before the start of this study and consequent tests after the study has started verified the viability of these devices, with little to no changes in scan angle, mirror reflectivity or resonant frequency (Figure 15). These devices continue to be under test for longer term data.
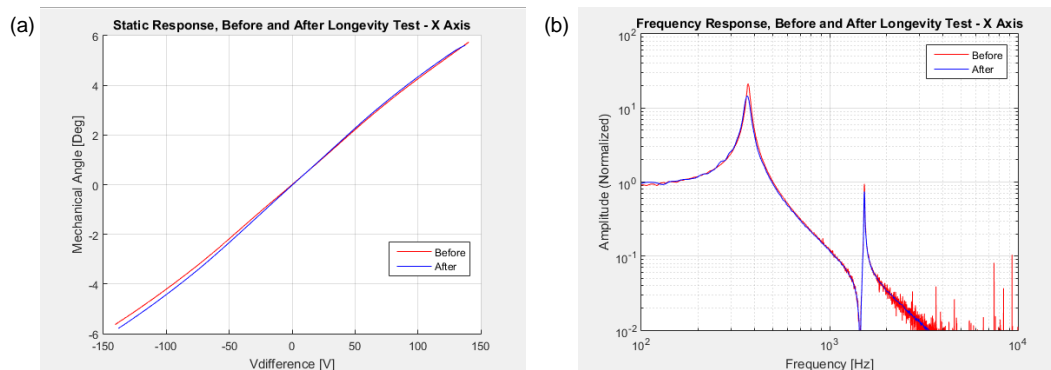

Figure 15. Characterization data of a single device, A8L1.1-5000AU, that has been measured before the start of a long term temperature study, and re-characterization after 2500 hours of sitting at 105°C. (a) The Static response and (b) Small Signal Frequency Response

5.4 MIRROR REFLECTIVITY AND POWER HANDLING

Mirrorcle MEMS mirrors come with two standard optical coatings of Aluminum (Al) and Gold (Au). Previously, a small number of R&D batches were coated with protected Silver (Ag) or other enhanced dielectric coatings; these coatings helped with reflectivity, but the mass of the coatings caused an undesirable, significant drop in the device's resonant frequency. The standard coating on Mirrorcle's mirrors is a thin layer of 60nm. Any dielectric coatings typically require thicknesses that are magnitudes larger (e.g. 100μm), which multiplies the mass of the mirror by a significant factor, and therefore drops the bandwidth and shock tolerance down to levels where the device cannot be used in most applications.

The standard coatings are able to handle ~2W of CW power in wavelengths from violet (405nm) to infrared, with certain wavelengths having higher thresholds due to the reflectivity characteristics of the specific coating. For example, a standard Al mirror with 2.0mm diameter has been shown to handle 4W of CW power at 450nm [6]. Application-specific package modifications can aid in removing heat from the mirror surface, increasing the device's damage threshold in higher power applications. The same Al mirror with 2.0mm diameter, with the package modifications for programmable light source application has been used without damage at up to 5.5W of CW power at 450nm. With Helium backfill, it is expected to operate at up to 17W of CW power, when mounted on room temperature assemblies. Larger bonded mirrors (e.g. 5mm in diameter) have been used at 8-10W in laser processing equipment (1064nm) without damage, owed to their significantly larger area for heat removal.

6. CONCLUSIONS

The learning control algorithms yielded excellent results, showing increases in bandwidth from running in open loop with only low pass filters at 0.5f to 1.5f, where f is the device's resonant frequency, after the training performed. These optimized waveforms were able to be downloaded to a controller, and scanned in open-loop, showing minimal error and excitation of the device's resonant frequency. The long-term behavior of the device with optimized scanning through ILC has also been ongoing, with over 1 billion cycles performed so far, with no change.

In all cases of devices studied, a high accuracy of optical scans is achieved, typically to within ±0.025° of nominal. Repeatability after training, then running in open loop is better than ±0.01° - however, this measurement was limited by the lower resolution of the position detecting sensor. Scan rates achieved vary based on mirror design, but in each case are greatly improved from those achievable with basic driving approaches. Each mirror demonstrated higher quality vector graphics content at faster refresh rates and stable linear rasters at rates below resonance where lines are scanned with uniform velocity. Additionally, each mirror could achieve stable fast rasters with the line-scanning axis rates just below resonance, giving sinusoidal scans with line rates of ~1.6f_{res}. Finally, each mirror was also demonstrated achieving rasters with rates above resonance, giving line rates of ~2.5f_{res}. In all of those cases the other axis could scan linear and sharp sawtooth or triangle waveforms. Based on the symmetry of the MEMS design, we demonstrated the same performance at different angles, e.g. rastering at a 45° angle.

The inherent robustness of the MEMS mirrors have also been demonstrated during this study. The integrated MEMS mirrors have all passed 1000G shock tests, and the 3.0mm mirrors have passed 500G shock tests. Devices have been characterized at a large range of temperatures (25°C to 195°C), showing successful operation and very small changes in angle/voltage relationship and resonant frequencies. Groups of devices have been thermally cycled at temperatures up to 105°C for several months with no changes in their performance or characterization. Further robustness tests are still on-going to gather more data.

7. REFERENCES

[1]   Moss, R., Yuan, P., Quesada, E., Sudharsanan, R., Stann, B., Dammann, J., Giza, M., and Lawler, W., "Low-cost compact MEMS scanning ladar system for robotic applications," Proc. SPIE 8379, 837903 (2012).

[2]   Stann, B. L., Dammann, J. F., and Giza, M. M., "Progress on MEMS-scanned ladar," Proc. SPIE 9832, 98320L (2016); doi: 10.1117/12.2223728.

[3]   Milanović, V., Kasturi, A., Yang, J., and Hu, F., "Closed-loop control of gimbal-less MEMS mirrors for increased bandwidth in LiDAR applications," Proc. SPIE 10191, 101910N (2017); doi: 10.1117/12.2264069.

[4]   "SpectroScan 3D MEMS LIDAR System Model MLS 201," Spectrolab Inc., Nov. 2012. Web. Jan. 2018. http://www.spectrolab.com/sensors/pdfs/products/SPECTROSCAN3D_RevA%20071912.pdf.

[5]   Petrick, D., Gill, N., Hassouneh, M., Stone, R., Winternitz, L., Thomas, L., Davis, M., Sparacino, P., and Flatley, T., "Adapting the SpaceCube v2.0 Data Processing System for Mission-Unique Application Requirements," Adaptive Hardware and Systems (AHS) 2015 NASA/ESA Conference, IEEE, 1-8 (2015).

[6]   Kasturi, A., Milanović, V., and Yang, J., "MEMS Mirror Based Dynamic Solid State Lighting Module," Journal of the Society for Information Display, Display Week 2016, May 2016.

[7]   Khanh, T.C., [12th International Symposium on Automotive Lightning – ISAL 2017 – Proceedings of the Conference: Volume 17], Herbert Utz Verlag, Darmstadt, 271-280 (2017).

[8]   Lu, C. D., Kraus, M. F., Potsaid, B., Liu, J. J., Choi, W., Jayaraman, V., Cable, A. E., Hornegger, J., Duker, J. S., and Fujimoto, J. G., "Handheld ultrahigh speed swept source optical coherence tomography instrument using a MEMS scanning mirror," Biomed. Opt. Express, 5(1), 293-311 (2014); doi: 10.1364/BOE.5.000293.

[9]   Nankivil, D., Waterman, G., LaRocca, F., Keller, B., Kuo, A. N., and Izatt, J. A., "Handheld, rapidly switchable, anterior/posterior segment swept source optical coherence tomography probe," Biomed. Opt. Express, 6(11), 4516–4528 (2015); doi: 10.1364/BOE.6.004516.

[10]   Shelton, R. L., Jung, W., Sayegh, S. I., McCormick, D. T., Kim, J., and Boppart, S. A., "Optical Coherence Tomography for advanced screening in the primary care office," J. Biophotonics, 7(7), 525-533 (2014); doi: 10.1002/jbio.201200243.

[11]   "Thorlabs – OCTH 900 Handheld OCT Scanner for 900 nm / 930 nm," Thorlabs. Web. Jan. 2018. https://www.thorlabs.com/thorproduct.cfm?partnumber=OCTH-900.

[12]   Giannini, J. P., York, A. G., and Shroff, H., "Anticipating, measuring, and minimizing MEMS mirror scan error to improve laser scanning microscopy's speed and accuracy," PLoS ONE, 12(10) (2017); doi: 10.1371/journal.pone.0185849.

[13]   "Hardware Guide," Mirrorcle Technologies, Inc., 25-35, Nov. 2016. Web. Jan. 2018. http://mirrorcletech.com/pdf/MTI_Hardware_Guide.pdf.

[14]   Milanović, V., "Linearized Gimbal-less Two-Axis MEMS Mirrors," 2009 Optical Fiber Communication Conference and Exposition (OFC'09), San Diego, CA, 25 Mar. 2009.

[15]   "Development Kits," Mirrorcle Technologies, Inc., Nov. 2016. Web. Jan. 2018. http://mirrorcletech.com/devkit.html.

[16]   "Iterative learning control," Wikipedia. Web. Jan. 2018.

[17]   Lee, K. S., Bang, S. H., and Chang, K. S., "Feedback-assisted iterative learning control based on an inverse process model," Journal of Process Control, 4(2), 77-89 (1994); doi: 10.1016/0959-1524(94)80026-X.

[18]   Wang, Y., Gao, F., and Doyle, F. J., "Survey on iterative learning control, repetitive control, and run-to-run control," Journal of Process Control, 19(10), 1589-1600 (2009); doi: 10.1016/j.jprocont.2009.09.006.

[19]   MIL-STD-883E Method-2002, "Test Method Standard – Microcircuits," 31 Dec. 1996. Dept. of Defense.

[20]   Moffatt, R. A., "Two-Dimensional Spatial Imaging Of Charge Transport In Germanium Crystals At Cryogenic Temperatures," Ph.D. Dissertation, Stanford University, Mar. 2016.

[21]   Moffatt, R. A., Cabrera, B., Kadribasic, F., Redl, P., Shank, B., Young, B. A., Brandt, D., Brink, P., Cherry, M., and Tomada, A., "Spatial imaging of charge transport in germanium at low temperature," Journal of Low Temperature Physics, 176(5-6), 943–951 (2014).

[22]   Milanović, V., "Improved Control of the Vertical Axis Scan for MEMS Projection Displays," 2007 IEEE/LEOS Optical MEMS and Their Applications Conf., Hualien, Taiwan, 12 Aug. 2007.

[23]   Overton, G., "Laser Lighting: White-light lasers challenge LEDs in directional lighting applications," Laser Focus World, 2 Feb, 2017, Web Jan, 2018.